Journal of Power Sources 188 (2009) 397–403

Contents lists available at ScienceDirect

Journal of Power Sources

journal homepage: www.elsevier.com/locate/jpowsour

Syntheses and catalytic performances of Ag–Ni bi-metals

Changlin Tang[a], Liping Li[a], Hongbo Gao[b], Guangshe Li[a,*], Xiaoqing Qiu[a], Jiang Liu[b]

[a] State Key Lab of Structural Chemistry, Fujian Institute of Research on the Structure of Matter, and Graduate School of Chinese Academy of Sciences, Fuzhou 350002, PR China
[b] School of Chemistry and Chemical Engineering, South China University of Technology, 381 Wushan Road, Guangzhou 510641, PR China

ARTICLE INFO

Article history:
Received 3 December 2008
Accepted 4 December 2008
Available online 9 December 2008

Keywords:
Ag–Ni bi-metals
Catalysis
Green syntheses
Fuel cell

ABSTRACT

Ag–Ni bi-metal nanocrystals were prepared by a novel solution method, in which ethanol was first taken as a green solvent with no use of any external toxic reducing agents. The as-prepared bi-metal nanocrystals were spherical and constructed by an aggregation of tiny crystals with particle size of about 12 nm. Infrared data indicated that the surfaces of the as-prepared nanocrystals were free of organic contaminants. The obtained bi-metal nanocrystals showed great potential as the additive in promoting the decomposition of ammonium perchlorate (AP), the key component of composite solid propellants. They were also initiated as the anode material of solid oxide fuel cells (SOFCs) which showed a maximum power density of 52.34 mW cm^{-2} for single cell at 800 °C.

© 2008 Elsevier B.V. All rights reserved.

1. Introduction

The ability to utilize more benign reagents and solvents derived from renewable sources is crucial to the green nanosyntheses [1] which can maximize the societal benefit while minimizing the negative impacts from waste, pollution, and hazards to human health that generate during the production and technological applications of nanoscale metals [2]. Transition metal nanocrystals are widely taken as model metallic catalysts and important components for nanoscale electronic device. When transition metals are used to decorate the noble metal nanocrystals or alloys, improved physical properties are expected. For instance, Pt–Ni, Ag–Ni bi-metals have shown superior electrochemical properties over pure noble metal or Ni metals for fuel cell uses. Though progress made in the preparation of nanoscale noble metals has been very impressive, the synthesis of noble-transition bi-metal nanocrystals is still very difficult, which generally requires rigorous conditions and/or highly toxic reducing agents to reduce the corresponding transition metal salts [1,3]. Consequently, green nanosynthesis of noble-transition bi-metals is still a challenge as to their future technological applications.

As well known, the reductive gases such as H_2 and CO are frequently used to reduce some metal salts to noble-transition bi-metal in the traditional metallurgy. These gases are however flammable and explosive. In this regard, one has to use two-step strategies: (1) formation of metal carbonyl cluster compounds by reacting metal salts with CO in methanol and ethanol solution, and (2) decomposition of thermally unstable metallo-organic precursors and noble metal salts complex to form the nanoscale noble-transition bi-metal/alloys [4]. The precursors for these purposes include $Fe(CO)_5$, $Co_2(CO)_8$ or $Ni(CO)_4$ which are generally very air sensitive and severely toxic. As a result, all handling has to be done in a glove box, and the final transition metal nanocrystals are usually highly defective and require significant annealing at elevated temperatures to produce high quality samples. The final material properties (e.g., saturated magnetic response) are typically only a small fraction of that found in the corresponding bulk counterparts [5]. Direct precipitation of noble-transition bi-metals nanocrystals from aqueous solutions is newly taken as an alternative route. Nevertheless, reduction of transition metals with highly negative reduction potentials always requires reducing agents like $NaBH_4$, $N_2H_4{\cdot}H_2O$, or $N_2H_4{\cdot}2HCl$ with considerably stronger reducing ability than that afforded by most amines, hydroxycarboxylic acids, or alcohols [6]. These reducing agents are either harmful or highly toxic, which inevitably bring chemical hazards to human health and the environment. Consequently, improved syntheses using more benign reagents and solvents especially those derived from renewable sources are highly needed, which allows the understanding of the synthetic chemistry of noble-transition bi-metal nanocrystals for their maximum benefit to society and the environment.

Ethanol is promising for such goals, since (1) it is a renewable agent that can be produced from the natural plants and (2) among all reducing agents, ethanol is least toxic to humans [7], though it has the α-hydrogen, common feature of alcohols for reducing ability, which is wildly employed to synthesize the noble metals. Nevertheless, ethanol was only the solvent in the conventional methods, which is still impossible to reduce the transition

* Corresponding author. Tel.: +86 591 83792846; fax: +86 591 83702122.
E-mail address: guangshe@fjirsm.ac.cn (G. Li).

0378-7753/$ – see front matter © 2008 Elsevier B.V. All rights reserved.
doi:10.1016/j.jpowsour.2008.12.011

metal ions because of the high redox potential of transition metal ions/metal [6]. It has to be stressed that more active polyalcohol is able to reduce some transition metal salt directly, but polyalcohol such as glycol is more expensive and the removal of organic remnant on the particle surface is not an easy work [8]. In this work, we explored the reduction of transition metal ions to form bi-metals in the presence of silver by ethanol. We proposed two steps to explain the formation of Ag–Ni nanoscale bi-metals and also studied the potential uses of the bi-metals in promoting the decomposition of ammonium perchlorate (AP) and as the anode materials for solid fuel cells.

2. Experiments

Chemicals of $AgNO_3$ (99% pure), $Ni(NO_3)_2{\cdot}6H_2O$ (99% pure), NaOH (99%), and ethanol (C_2H_5OH) (99% pure) were purchased from Shanghai Guoyao Chemical Company and utilized as the starting materials for all sample syntheses. A typical procedure for the sample synthesis is described as follows: 0.1 mmol $AgNO_3$ and 9.9 mmol $Ni(NO_3)_2{\cdot}6H_2O$ were dissolved in 100 mL ethanol, into which a mixed solution of 50 mmol NaOH and 50 mL ethanol was slowly added to get a suspension while stirring. The mixed suspension was transferred to two-100 mL Teflon-lined stainless steel autoclaves (with a filling degree of 70%), which were allowed to react at 180 °C for 2 h in an oven. After cooling to room temperature, a black product was washed with de-ionized water or 25 wt% ammonia solution for several times, and dried at 60 °C in air. The final products were named as Ag_xNi_{1-x}, where x denotes the initial ratio of Ag to Ni.

Phase purities of the as-prepared samples were characterized by X-ray diffraction (XRD) on Rigaku DMAX2500 X-ray diffractometer using a copper target. The average crystallite size, D, was calculated from the diffraction peak (1 0 1) using the Scherrer formula:

$$D = \frac{0.9\lambda}{\beta \cos\theta} \quad (1)$$

where λ(=1.5418 Å) is the X-ray wavelength employed, θ is the diffraction angle, and β is defined as the half-width after subtracting the instrumental broadening. Sample morphologies and particle sizes were determined using transmission electron microscopy (TEM) on a JEM-2010 apparatus with an acceleration voltage of 200 kV. Samples for TEM were prepared by making a dispersion of the samples in ethanol and putting drops of them on carbon-coated copper grids. The particle size distribution of the samples was calculated by counting 100 separated particles at 10 times in diameter with magnifier from the TEM photograph. The magnetization curve was recorded at room temperature using a Quantum Design PPMS-7 magnetometer. The infrared spectra were measured on a Perkin-Elmer IR spectrophotometer. A KBr pellet technique was used for the powder samples. BET-specific surface areas of the samples were determined by N_2 adsorption isotherms at 77 K on a Micromeritics ASAP 2000 surface area and porosity analyzer.

The catalytic roles of bi-metal nanocrystals in the thermal decomposition of AP (180 μm) were studied by thermogravimetric analysis (TG) and differential scanning calorimeter (DSC) in N_2 atmosphere over the temperature range of 30–500 °C. The heating rate was fixed at 10 °C min^{-1}. AP and bi-metal sample were mixed at a mass ratio of 98:2 to prepare the target samples for thermal decomposition analyses. A total sample mass of 20 mg was used for all runs [9].

The bi-metal nanocrystals were also investigated as the anode materials of solid oxide fuel cell (SOFC). Electrochemical activity was examined using a CHI604B electrochemical workstation (Shanghai Chenhua Instruments Ltd., Shanghai, China) in the temperature range from 550 to 800 °C. Eight mole percentage yttria-stabilized zirconia pellet (thickness = 0.6 mm) was used as the electrolyte of SOFC single cell. Ag–Ni bi-metal nanocrystals and YSZ powders with a mass ratio of 7:3 were mixed thoroughly and used as the anode materials. The mixture of $La_{0.8}Sr_{0.2}MnO_3$ and YSZ powders (donated by Building Material Academy of China, Beijing, China) with a mass ratio of 1:1 (v/v) is served as the cathode material. The particle sizes of $La_{0.8}Sr_{0.2}MnO_3$ and YSZ powders are several micrometers [10a]. The surface area of the cell is 0.2 cm^2, details for the assembling single cell could be found elsewhere [10]. During the single cell measurements, hydrogen gas (99.99%) produced by a CH2500 hydrogen generator was fed into the alumina tube as fuel and the flow rate was 200 ml min^{-1}, while oxygen in air was used as the oxidant. The current–voltage (I–V) curves are tested by linear sweep voltammetry at a scanning rate of 5 mV s^{-1}.

3. Results and discussion

XRD pattern of the sample with Ag/Ni = 1/99 prepared at 180 °C is shown in Fig. 1. Data analysis indicates that the as-prepared sample Ag_1Ni_{99} has a dominant component of Ni metals, which is indicated by the strong characteristic diffraction peaks at 44.5°, 51.8°, and 76.4° for Ni (1 1 1), (2 0 0), and (2 2 0), respectively. Traces of minor components are Ag and $Ni(OH)_2$ which are characterized by a broad peak at 38.1° and two weak peaks at 33° and 52.1°. $Ni(OH)_2$ was completely removed by ammonia water washing (Fig. 1, top). Though the initial atomic ratio of Ag to Ni is only 1:99, strong peaks for Ag are discernable in the final products Ag_1Ni_{99} (Fig. 1). This phenomenon may be originated from three factors: firstly, noble atoms Ag has larger diffraction factors than atom Ni, so the signal of Ag strengthens in XRD. Secondly, the ratio of Ag to Ni metals in Ag_1Ni_{99} is not exactly the same as that in the precursors. As determined by inductively coupled plasma (ICP) measurement on Ag_1Ni_{99}, the ratio of atoms Ag to Ni are 1:95.2 and 1:86.4 before and after ammonia washing, respectively. Thirdly, phase diagram of Ag/Ni shows that metals Ag and Ni are immiscible over the entire composition range; so metal Ag and Ni should be metals rather than Ag–Ni alloys [11]. Using Scherrer formula for Ag(1 1 1), the crystallite size is 3.7 nm. Nevertheless, it is still very difficult to find Ag particles in the HRTEM images because of the low content of Ag in Ag_1Ni_{99}. For Ni(1 1 1), the crystallite size of the as-prepared Ni was calculated to be approximately 12 nm, which is about three times smaller than that observed by TEM (Fig. 2a and c). The as-prepared samples are apparently spherical and are constructed by an aggregation of tiny

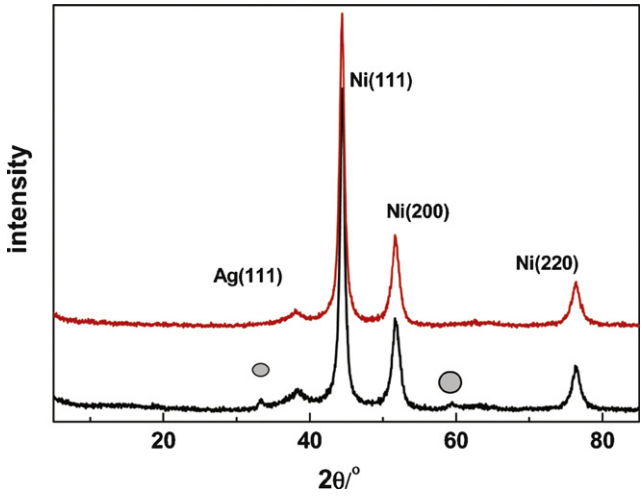

Fig. 1. XRD pattern of the as-prepared sample (bottom) with an initial molar ratio of Ag:Ni = 1:99, and that after ammonia washing (top). Symbol (●) represents the trace of impurity $Ni(OH)_2$.

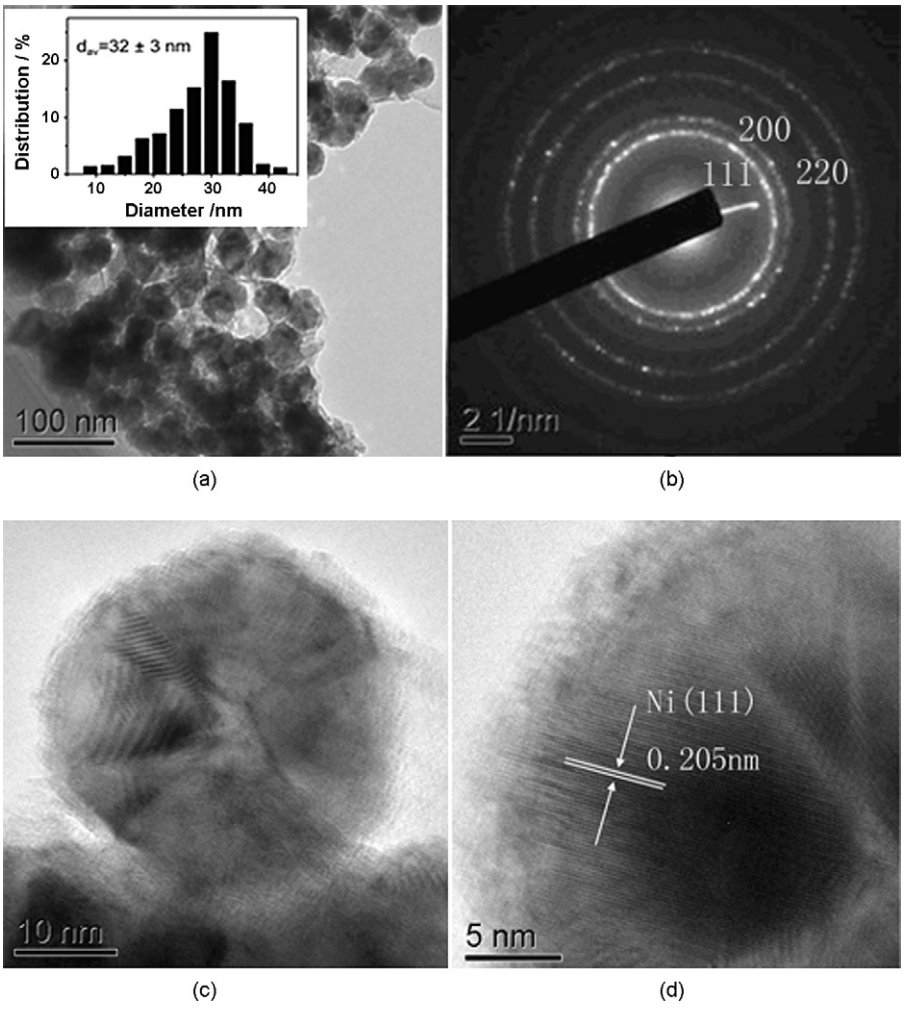

Fig. 2. (a) TEM images of the as-prepared sample Ag_1Ni_{99}, the size distribution histogram is illustrated in the inset. (b) SEAD with diffraction cycles of metal Ni(1 1 1), (2 0 0), (2 2 0), which is consistent with the close image of (c) and (d) that the spherical particle are packed with small nanometal particles. HRTEM shows the Ni(1 1 1) lattice face with d = 0.205 nm.

crystals (Fig. 2c). The regularity of lattice planes in the HRTEM image (Fig. 2d) clearly indicates that the spacing of the adjacent planes is about 0.205 nm which corresponds to that for Ni(1 1 1). Selected-electron area diffraction (SEAD) measurement further confirms the metal nickel crystals (Fig. 2b), which are composed of multi-crystal particles as characterized by the circle-like diffraction points. The specific surface area of the samples was 36.2 $m^2\,g^{-1}$ as is determined by BET (Fig. S1). Assuming perfect spheres without any internal pores in Fig.S1, i.e., BET ($m^2\,g^{-1}$) = $6/d/\rho$, where d is the particle diameter and ρ = 6.7 g cm^{-3} is the density of bulk Ni, the particle size should be 24 nm. But the BET area for 12 nm Ni should be 74 $m^2\,g^{-1}$, about twice larger than that by experimental observation. This further illustrates that the XRD diameter is not the overall particle diameter. Therefore, the size distribution of Ag_1Ni_{99} is mainly around 32 nm (inset of Fig. 2a).

Ag_1Ni_{99} nanocrystals prepared using this method are pure without any organic contaminants left at the particle surfaces as confirmed by FT-IR measurements, while other organic contaminants like polyalcohol are always adsorbed on the particle surfaces [8] once polyalcohol are employed for sample synthesis. IR spectra of the as-prepared sample Ag_1Ni_{99} and ammonia washed product are given in Fig. 3. The vibrations detected at 3641 and 516 cm^{-1} for the as-prepared sample (Fig. 3a) are attributed to the vibration mode of OH^- for impurity $Ni(OH)_2$, which can be removed completely by ammonia washing (Fig. 3b). Vibrations observed at 3400 and 1637 cm^{-1} are contributed from the absorbed water, and that at 1440 cm^{-1} corresponds to the vibration of carbonate species. The absence of the peaks around 2800 cm^{-1} for ν-C–H suggested that the surface of the as-prepared metal particles were free of organic

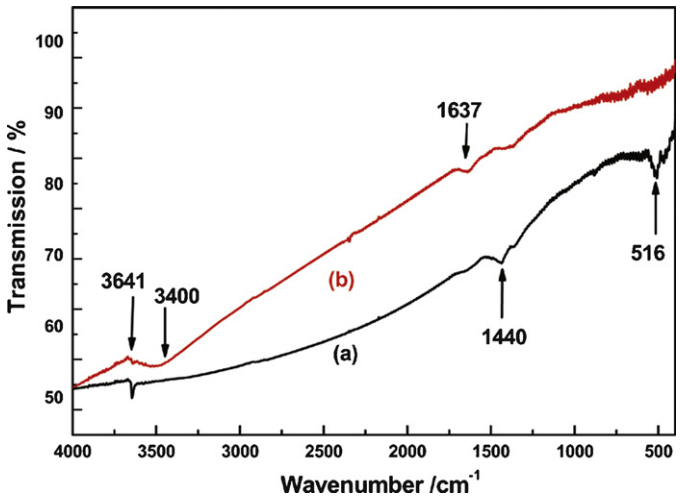

Fig. 3. FT-IR spectrum of the as-prepared sample Ag_1Ni_{99} (a) and that after ammonia washing (b) to remove the minor $Ni(OH)_2$ impurity.

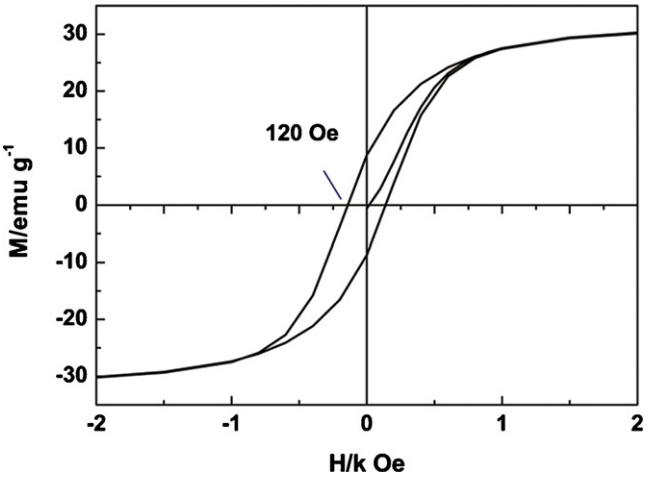

Fig. 4. Magnetization curve of Ag_1Ni_{99} measured at room temperature. The coercive force is H_C = 120 Oe and the saturated magnetic moment is about M_S = 32 emu g^{-1}.

species. Therefore, by using ethanol as solvent, the silver–nickel bi-metal nanoparticles are free of organic residuals on the surfaces.

The as-prepared bi-metal nanocrystals showed strong room temperature ferromagnetism (Fig. 4). The magnetization data tends to saturate under a low magnetic field of H = 2 kOe. The saturation magnetization is Ms = 32 emu g^{-1}, which is slightly smaller than that of Ms = 55 emu g^{-1} for bulk Ni metal. This observation can be understood in terms of the particle size effect [12a], since as stated above, the crystallite size of the as-prepared Ni was only about 12 nm which may give rise to a smaller Ms [12]. Surprisingly, as indicated in Fig. 4, the coercive force of the as-prepared Ni nanocrystals is H_C = 120 Oe, which is larger than that of H_C = 100 Oe for bulk Ni metal. Because the aggregation of small crystals (Fig. 2c and d) can enhance the magnetic interaction of the surface moments [13]. It is noteworthy to point out that the paramagnetic Ag should be effective to enhance the H_C of ferromagnetic Ni [12d] through the interface interaction, but this contribution could be neglected for the low atomic ratio of Ag in Ag_1Ni_{99}. Therefore, size effect should dominate the magnetic variation when the size of metal Ni is in the nanoscale [12a].

It is well known that Ag^+ can be easily reduced to metal Ag, because the possible component oxides like Ag_2O could be precipitated from silver salt solution, and because Ag_2O is prone to decompose due to a positive standard electrode potential of φ = 0.35 V for Ag_2O/Ag [14b]. Comparatively, when $Ni(OH)_2$ was formed in basic solutions, the reduction reaction of $Ni(OH)_2$/Ni gives a negative value φ = −0.72 V vs. standard hydrogen electrode at pH 14. Also, this potential is 110 mV positive more than the H_2/H^+ potential in the same solution (i.e., +0.11 V positive vs. the reversible hydrogen electrode potential), which means that ethanol is thermodynamically able to reduce $Ni(OH)_2$ to Ni. Because ethanol oxidation potential is within 50 mV of H_2/H^+ potential, i.e., within 50 mV reversible Hydrogen Electrode [14]. The reduction of $Ni(OH)_2$ to Ni metal by ethanol is allowed thermodynamically. It is still impossible to ignite this reaction directly. Then, what governed the reduction reaction of Ni^{2+} to Ni? To explore the relevant reduction mechanism, we did several parallel experiments. Fig. 5 shows the XRD patterns of the relevant products. From Fig. 5, it is found that: (i) when ethanol was replaced by water, the product was consisted of β-$Ni(OH)_2$ and Ag (Fig. 5a); (ii) when no NaOH solution was involved, we obtained a mixture of α-$Ni(OH)_2$ and Ag (Fig. 5b). It is thus obvious that OH^- plays an important role in the reduction reaction; (iii) when no Ag/Ag^+ species was involved, the product was pure β-$Ni(OH)_2$ (Fig. 5c), which implied that the existence of Ag reduced the potential barrier of reaction from $Ni(OH)_2$ to Ni; (iv)

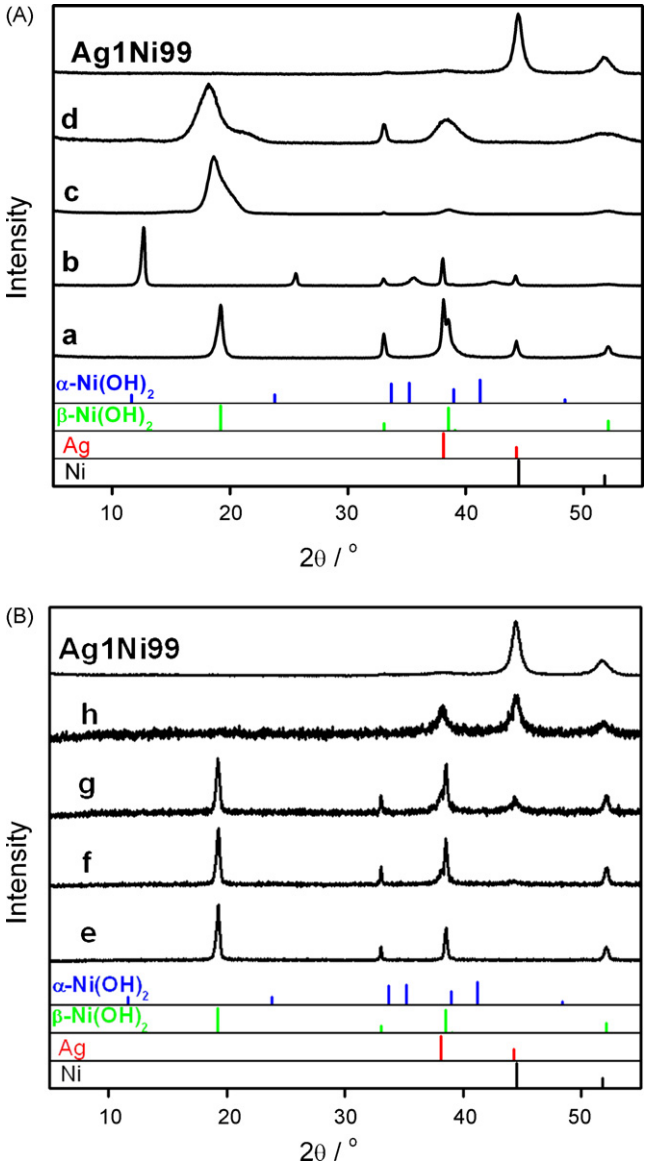

Fig. 5. XRD patterns of the samples synthesized under different reaction conditions: (A) in the absence of ethanol (a), NaOH (b), $AgNO_3$ (c), and low temperature of 130 °C (d); (B) by using $Ni(OH)_2$ and Ag as starting materials to react at 180 °C for 0 min (e), 30 min (f), 60 min (g), and 120 min (h). All the products are samples without ammonia water washing. The vertical bar below the patterns are the standard data for Ni, Ag, α-$Ni(OH)_2$, and β-$Ni(OH)_2$, and the product of Ag_1Ni_{99} (bottom of Fig. 1) is also shown for comparison.

when the reaction temperature is lower than 130 °C (Fig. 5d), the product was β-$Ni(OH)_2$ mixed with Ag, which seems to be consistent with the strong temperature dependence of Ag catalytic activity for the ethanol oxidation into acetic acid [15]; (v) when the starting materials were $Ni(OH)_2$ or $AgNO_3$ instead of nickel and silver salts, nanometal Ni can also be prepared, though the reaction time has to be significantly increased and more $Ni(OH)_2$ would be formed comparing with that when using $AgNO_3$ and $Ni(NO_3)_2$ as the starting material (Fig. 5e–h and Ag_1Ni_{99}, Table S1). In this dynamic study, the ratio of atomic Ag to Ni was 1:9 in the reaction precursors, so peak of Ag(1 1 1) near 38° can be discerned after heat treatment for 30 min (the arrow in Fig. 5B(f)). When heat treatment for 60 min, the peak of Ag(1 1 1) strengthens, but strong peaks of $Ni(OH)_2$ at 18° still exist which means that the reduction of $Ni(OH)_2$ is neglectable. At 120 min, the peak at 18° disappears and strong peak of Ni(1 1 1) occurs, but the crystallization could be very poor.

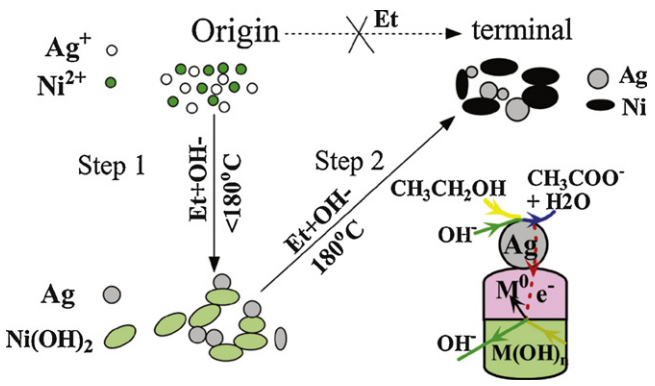

Scheme 1. Synthetic strategy proposed for Ag–Ni nanoscale bi-metals in the presence of ethanol: Step 1 represents the transformation of Ag^+ and Ni^{2+} to Ag and $Ni(OH)_2$ under alkaline condition, while Step 2 corresponds to the reduction of $Ni(OH)_2$ to Ni by ethanol. The catalytic role of Ag in the formation reaction of Ni metal is schematically shown.

However, when using $AgNO_3$ and $Ni(NO_3)_2$ as the staring materials, $Ni(OH)_2$ and Ag firstly formed with NaOH addition could be mixed uniformly at the nanoscale level and contact each other to promote the redox reaction to Ag–Ni bi-metal nanocrystals (Fig. 5B Ag_1Ni_{99}). Here Ni nanoparticle are highly crystallized though the reaction conditions are the same as that using $Ni(OH)_2$ precursor.

Bearing these results in mind, we proposed a strategy to explain the formation of Ni metal in the presence of ethanol. As illustrated in Scheme 1, noble metal ions are directly reduced to noble metals (e.g., Ag) by ethonal under alkaline condition (Step 1), as that in the conventional synthesis of noble metal at elevated temperatures. At the meantime, transition metal ions are also percipitated to form metal hydroxides that may contact with the freshly reduced noble nanometals. Consequently, in the Step 2, these noble metals may act as the catalyst to initiate the oxidation reaction of ethonal and reduction of transition metal hydroxide as well [15]. This step is key to the formation of noble-transition bi-metals. To realize the catalytic oxidation of ethonal on noble metal crystals, it is suitable to use alkaline condition, in which ethonal could be deeply oxidized to CH_3COO^- and/or CO_2 at elevated temperatures [15]. Based on these analyses, the reaction at the presence of noble metal catalyst Ag (Step 2, Scheme 1) may proceed as follows [16]:

$$CH_3CH_2OH + 5OH^- \xrightarrow{Ag} CH_3COO^- + H_2O + 4e^-$$

Electrons are thus released from the oxidation of ethanol in the presence of catalyst Ag, which are transferred to $Ni(OH)_2$ to activate the reduction of the transition metal hydroxide contacted with metal Ag via the following path:

$$Ni(OH)_2 + 2e^- \rightarrow Ni + 2OH^-$$

Finally, the noble-transition bi-metal nanocrystals are produced.

From the work principle proposed in Step 2 of Scheme 1, the ethanol oxidation to acetic acid is necessary for the complete redox reaction. The ethanol oxidation was examined by infrared and ion trap mass spectra. From the FT-IR spectra (Fig. 6), the pre-reaction solution showed the simply mixed absorptions from nitrate and ethanol species. When the formation reaction was ended, two new absorptions of the reaction residual were observed at 1415 and 1575 cm^{-1}, which can be attributed to the typical absorptions of symmetric and un-symmetric stretch vibration of C=O bonding. The residual solution did not present any characteristic absorption peaks for C=O at 1728 cm^{-1} or for C–O–C un-symmetric stretching vibration at 1256 cm^{-1} for ethyl acetate. These observations indicate that ethyl acetate was not generated during the reactions. The absorptions associated with the NO_3^- species at 825 and 1764 cm^{-1}

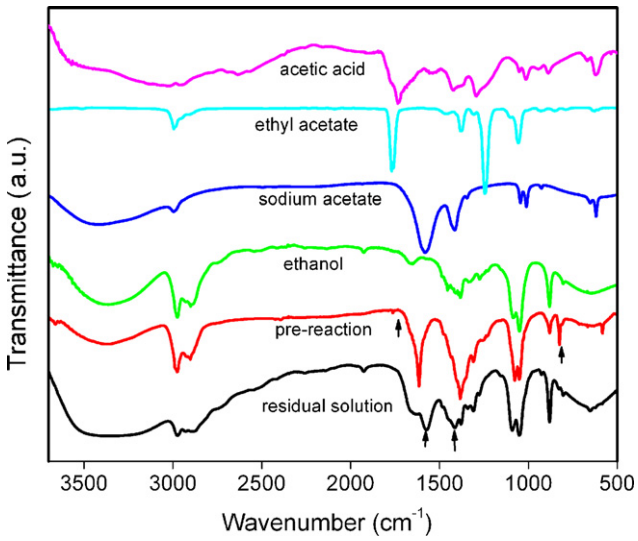

Fig. 6. FT-IR spectra of the pre-reaction solution and reaction residual solution, which are compared with the possible by-products like ethanol, sodium acetate, acetic acid and ethyl acetate.

were apparently weakened. Thus, part of NO_3^- ions were exhausted because of the following reaction [9]:

$$4CH_3CH_2OH + NO_3^- \rightarrow 4CH_3CHO + NH_3 \uparrow + OH^- + 2H_2O$$

The compounds with C=O group are attributed to CH_3COO^- as indicated by ion trap mass spectrum analysis (Fig. S2). Therefore, with the catalyst Ag, ethanol oxidation accompanied with the Ni^{2+} reduction becomes the center pertinent to the formation of Ag–Ni nanocrystals.

The as-prepared Ag_1Ni_{99} bi-metals were explored as an additive to the thermal decomposition of AP, the key component of composite solid propellants. The roles of Ag_1Ni_{99} in the thermal decomposition of 100 μm AP (Fig. S3) were investigated by TG and DSC measurements in an open lid with a total mass of 20 mg. The results are presented in Fig. 7. The thermal decomposition of pure AP, depending on the crystal quality, usually undergoes two or more steps. For the pure AP used in the present work, two mass losses were observed, as indicated by two peaks at 328 and 420 °C in the first derivative curve of raw TG data (Fig. 7). Therefore, the thermal decomposition proceeded in two steps: the first step started at about 290 °C, which corresponds to the low-temperature decom-

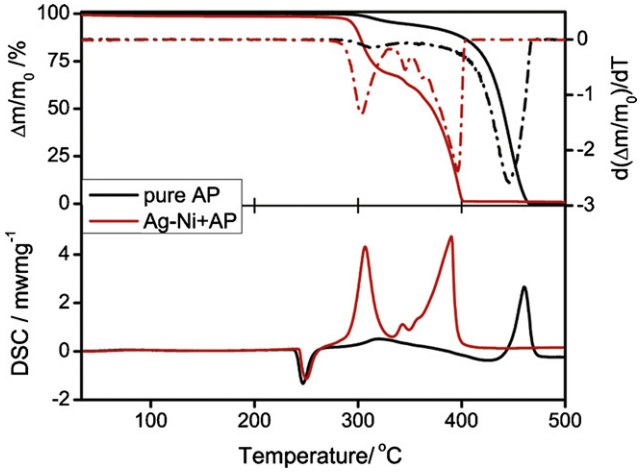

Fig. 7. TG (top) and DSC (bottom) curves of pure AP and AP with 2% Ag_1Ni_{99} additive in mass. The dash lines represent the first derivative curve of the raw TG data.

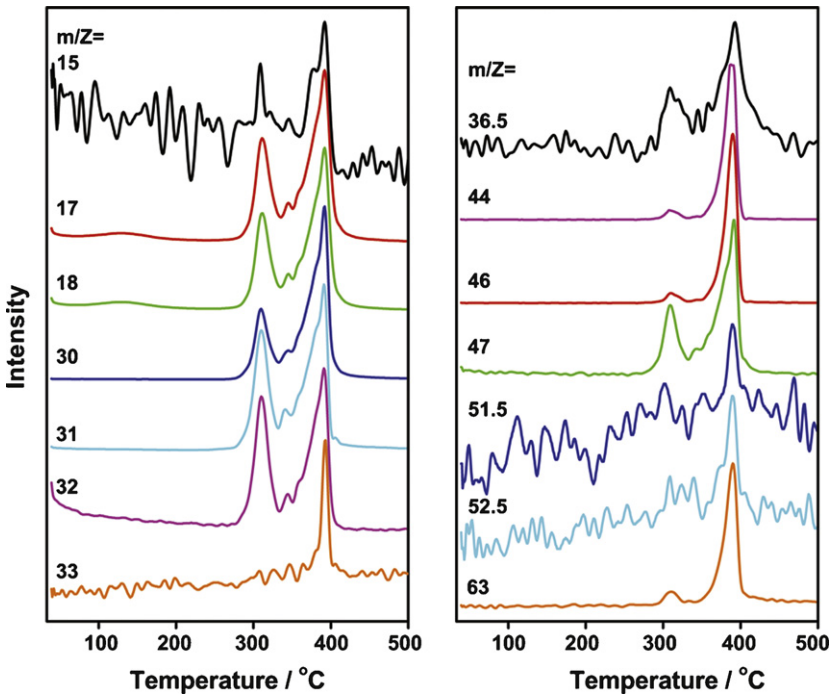

Fig. 8. Quadrupole mass spectra of AP with 2 wt% Ag_1Ni_{99} additive. The signals with m/z = 15 (NH), 17 (OH or NH_3), 18 (H_2O), 30 (NO), 31 (HNO), 32 (O_2), 33 (H_3NO), 36.5 (HCl), 44 (N_2O), 46 (NO_2), 47 (HNO_2), 51.5 (ClO), 52.5 (HOCl), and 63 (HNO_3) were observed.

position (LTD), while the second step starting at about 350 °C is associated with the high-temperature decomposition (HTD). These two steps were also indicated in the corresponding DSC curves as characterized by two exothermic peaks at about 320 and 460 °C. The endothermic peak at 240 °C is due to the crystal transformation of AP from orthorhombic to cubic phase.

When AP was mixed with bi-metal Ag_1Ni_{99}, the decomposition temperature for both LTD and HTD processes reduced to 307 and 390 °C. From DSC curves (bottom of Fig. 7), it is found that the heights of two exothermic peaks are near the same. Comparing to a broad exothermic peak related to LTD process for pure AP, the sharp peak inclined that the LTD process is accelerated by addition of bi-metal Ag_1Ni_{99}. In addition to the LTD and HTD exothermic peaks, a weak exothermic peak was also observed at 343 °C. Considering the absence of this fine thermal effect in AP decomposition with nanometal Ag or nano-oxide NiO as additives (Fig. S4), this new peak should be associated with the presence of Ni metal.

Previous literature has indicated that metals and metal oxide nanoparticles could improve the burning rates of AP [16,17]. For pure AP, LTD involves a heterogeneous process which includes a proton transfer in the AP subsurface to yield NH_3 and $HClO_4$, the adsorption of NH_3 and $HClO_4$ in the porous structure, and finally the decomposition of $HClO_4$ and reaction with NH_3. Alternatively, HTD involves the simultaneous dissociation and sublimation of AP to $NH_{3(g)}$ and $HClO_{4(g)}$ [17]. To understand the reaction mechanism why bi-metal Ag_1Ni_{99} accelerates the AP decomposition, the burning gas was analyzed by quadrupole mass spectrum. As indicated in Fig. 8, certain gases were released during these two processes, consistent with TG and DSC measurements. Signals were observed at m/z = 18 for H_2O and 32 for O_2 during LTD process, which indicates that $HClO_4$ was desorbed from AP crystal and decomposed partly. The released oxygen, on the one hand, reacted with NH_3 to form nitrogen oxides N_2O at m/z = 44, NO at m/z = 30, and NO_2 at m/z = 46. Bi-metal Ag_1Ni_{99} nanoparticles were also oxidized to give metal oxide which stimulated the HTD process. In the HTD process, NH_3 was thoroughly oxidized to produce HNO_3 (m/z = 63) and the relevant compounds (m/z = 33, 36.5, etc.). Compared with NiO additive (Fig. S4), the addition of bi-metal Ag_1Ni_{99} did not eliminate the HTD. Basing on the DSC measurement of bi-metal Ag_1Ni_{99}, however, the total released heat was 1253 J g^{-1}, which is slightly larger than that of NiO (1220 J g^{-1}).

As well known, Ni metal could be used as anode of SOFC. The electrochemical activity of Ag–Ni bi-metal nanocrystals was examined by SOFC single cell. The obtained output performance is shown in Fig. 9. The open-circuit voltage (OCV) at 550 °C was 1.074 V. When the temperature increased to 800 °C, OCV was reduced to 0.997 V, which is caused by temperature effect as indicated by Nernst equation for the reaction of $H_2 + ½O_2 = H_2O$:

$$E = E^0 + \frac{RT}{2F}\ln\left(\frac{P_{H_2}P_{O_2}^{1/2}}{P_{H_2O}}\right)$$

where E^0 is the electromotive force (EMF) at standard pressure, F is Faraday constant. P_{H_2}, P_{O_2} and P_{H_2O} are the partial pressure of

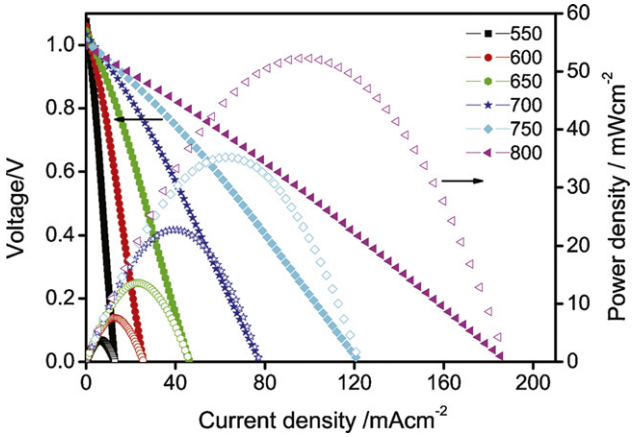

Fig. 9. Output performance of SOFC operated with anode Ag_1Ni_{99} bi-metals at temperature from 550 to 800 °C.

hydrogen, oxygen and water in bar. Because of the negative value for the second term, increase temperature would result in a decrease in EMF. From Fig. 9, it can be seen that power density increased with temperature. At 800 °C, the maximum power density was 52.34 mW cm^{-2}, which is lower than the micrometer Ni–YSZ electrode in our previous work [10]. The increase of power density with temperature is related to the enhanced O^{2-} ion conduction of the YSZ electrolyte.

4. Conclusions

Ethanol was initiated as the reductant to the green nano-syntheses of novel Ag–Ni bi-metal nanocrystals. The reduction reaction of Ni^{2+} to Ni was ascribed to the enhancement of ethanol activity at the presence of silver. As indicated by TEM and HRTEM observations, the as-prepared nanocrystals are spherical and constructed by an aggregation of tiny crystals with particle size about 12 nm. The bi-metal nanocrystals are free of organic contaminants on surfaces and showed strong room-temperature ferromagnetism. When using as the additive, the as-prepared Ag–Ni bi-metals reduced the decomposition temperature of AP. The Ag–Ni nanocrystals can also be used as anode materials of SOFC, which showed a maximum power density of 52.34 mW cm^{-2} at 800 °C.

Acknowledgments

This work was financially supported by NSFC under the contract (nos. 20773132, 20771101, 20831004), National Basic Research Program of China (nos. 2007CB613301, 2009CB939801), and Directional program of Chinese Academy of Sciences (KJCXZ-YW-M05).

Appendix A. Supplementary data

Supplementary data associated with this article can be found, in the online version, at doi:10.1016/j.jpowsour.2008.12.011.

References

[1] J.A. Dahl, B.L.S. Maddux, J.E. Hutchison, Chem. Rev. 107 (2007) 2228.
[2] (a) M. Kidwai, V. Bansal, A. Saxena, A. Shankar, R. Shankar, S. Mozumdar, Tetrahedron Lett. 47 (2006) 4161;
(b) O.V. Yazyev, A. Pasquarello, Phys. Rev. Lett. 100 (2008) 156102;
(c) C. Burda, X.B. Chen, R. Narayanan, M.A. El-Sayed, Chem. Rev. 105 (2005) 1025;
(d) R. Ferrando, J. Jellinek, R.L. Johnston, Chem. Rev. 108 (2008) 845.
[3] A. Roucoux, J. Schulz, H. Patin, Chem. Rev. 102 (2002) 3757.
[4] J.P. Wilcoxon, B.L. Abrams, Chem. Soc. Rev. 35 (2006) 1162.
[5] (a) S.R. Hoon, M. Kilner, G.J. Russell, B.K. Tanner, J. Appl. Polym. Sci. 10 (1966) 1915;
(b) C.H. Griffiths, M.P. O'Horo, T.W. Smith, J. Appl. Phys. 50 (1979) 7108;
(c) P. Hess, P.J.R. Parker, J. Appl. Polym. Sci. 10 (1966) 1915.
[6] B.L. Cushing, V.L. Kolesnichenko, C. O'Connor, J. Chem. Rev. 104 (2004) 3893.
[7] see: http://people.uis.edu/gtram1/organic/alcohols/oxidation.htm.
[8] M. Zawadzki, J. Alloys Compd. 454 (2008) 347.
[9] X.F. Sun, X.Q. Qiu, L.P. Li, G.S. Li, Inorg. Chem. 47 (2008) 4146;
L.P. Li, X.F. Sun, X.Q. Qiu, J.X. Xu, G.S. Li, Inorg. Chem. (2008), doi:10.1021/ic8008283;
L.J. Chen, G.S. Li, L.P. Li, J. Therm. Anal. Calor. 92 (2008) 765;
L.J. Chen, L.P. Li, G.S. Li, J. Alloys Compd. 464 (2008) 532.
[10] (a) J. Ding, J. Liu, J. Am. Ceram. Soc. 91 (2008) 3303;
(b) H.B. Gao, J. Liu, H.Y. Chen, S. Li, T.M. He, Y. Ji, J.D. Zhang, Solid State Ionics 179 (2008) 1620.
[11] E. Cottancin, M. Gaudry, M. Pellarin, J. Lerme, L. Arnaud, J.R. Huntzinger, J.L. Vialle, M. Treilleux, P. Melinon, J.L. Rousset, M. Broyer, Eur. Phys. J. D 24 (2003) 114.
[12] (a) W. Gong, H. Li, Z.G. Zhao, J.C. Chen, J. Appl. Phys. 69 (1991) 5119;
(b) D.H. Chen, C.H. Hsieh, J. Mater. Chem. 12 (2002) 2412;
(c) S.H. Wu, D.H. Chen, J. Colloid Interf. Sci. 259 (2003) 282;
(d) L. Wang, J. Lou, Q. Fan, M. Suzuki, I. Suzuki, M. Engelhard, Y. Lin, N. Kim, J. Wang, C. Zhong, J. Phys. Chem. B 109 (2005) 21593.
[13] C. Rath, K.K. Sahu, S.D. Kulkarni, S. Anand, S.K. Date, R.P. Das, N.C. Mishra, Appl. Phys. Lett. 75 (1999) 4171.
[14] (a) M. Taibi, S. Ammar, N. Jouini, F. Fievet, P. Molinie, M. Drillon, J. Mater. Chem. 12 (2002) 3238;
(b) J.A. Dean, Lange's Handbook of Chemistry, 15th edition, McGraw-Hill, New York, 1999.
[15] (a) Y. Shiraishi, N. Toshima, Colloids Surf. A 169 (2000) 59;
(b) V.R. Gangwal, J. van der Schaaf, B.F.M. Kuster, J.C. Schouten, J. Catal. 229 (2005) 389.
[16] (a) Dicks, L. Andrew, Curr. Opin. Solid State Mater. Sci. 8 (2004) 379;
(b) J.M. Skowronski, A. Wazny, J. Solid State Electrochem. 9 (2005) 890.
[17] (a) P. Erhart, A. Klein, K. Albe, Phys. Rev. B 72 (2005) 825213;
(b) V.V. Boldyrev, Thermochim. Acta 443 (2006) 1;
(c) D.L. Reid, A.E. Russo, R.V. Carro, M.A. Stephens, A.R. LePage, T.C. Spalding, E.L. Petersen, S. Seal, Nano Lett. 7 (2007) 2157.